JOURNAL OF MATERIALS SCIENCE **34** (1999) 5477–5487

Coherency strains influence on martensitic transformation of γ-Fe particles in compressed Cu-Fe alloy single crystals

A. M. WUSATOWSKA-SARNEK*, H. MIURA, T. SAKAI
Department of Mechanical and Control Engineering, The University of Electro-Communications, Chofu, Tokyo 182-8585, Japan
E-mail: sarnek-a@fedu.uec.ac.jp

Single crystals of a Cu-Fe alloy, which contained spherical γ-Fe particles, were compressed up to shear strain of 0.17 in liquid nitrogen bath. In the process of straining the structural (optical and TEM) observations in as-deformed and post-deformation annealed samples were provided. The substructure of deformed samples was characterized by slightly developed cell structure and lack of distinct layer-like arrangements of dislocations. Three kinds of particles were found: coherent and semi-coherent f.c.c. γ-Fe and martensiticly transformed b.c.c. α-Fe. The critical diameter for coherency loss was found to be 58 nm at the initial stage of deformation decreasing with strain to 50 nm. These values coincided with the theoretical estimations. It was suggested that relaxation of coherency strains around γ-Fe particles by the generation of interface dislocations might occur prior to the martensitic transformation. This assumption might explain the particle size dependency of martensitic transformation.

1. Introduction

Aging of solution-treated Cu-Fe alloy results in the precipitation of γ-Fe particles of excellent coherency with matrix due to the small lattice misfit between Cu and Fe. Such metastable precipitates do not transform to the α-Fe ones on cooling, even down to the liquid helium temperature [1]. We may come to think why martensitic transformation (MT) of γ-Fe particles does not occur by simple cooling which is on contrary to the sample of bulk austenite. The variation of γ-Fe and α-Fe phase free energy with temperature is the driving force for transformation and this does not depend on the geometry of sample. Thus the particle is kept in the metastable position by matrix constrains. If the transformation process is related with the coherency strains, it should be easier when the coherency strains become lower. The extreme case is an elimination of strains by extraction of precipitates from the matrix, which cause automatic transformation [2]. Lowering strains can be achieved by either loss of coherency or lowering the misfit strain by homogenizing the lattice types. Indeed, there exist in the literature experimental evidences supporting above suppositions. The basic strain lowering methods leading to the MT of particles conducted on the Cu-Fe alloy may be cited as follows:

(1) Coherency loss during ion bombardment by introducing static dislocation loops of vacancy type or stacking fault thetraedra at the vicinity of particles [3, 4].

(2) Weakening coherency strains during particle growth. Larger particles (diameter $>$ 200 nm) obtained by the long time annealing transform by simple cooling [5].

(3) Lowering the misfit strain ε by decreasing temperature due to the different thermal expansion coefficient of Cu and Fe lattice. Lowering temperature from 300 to 77 K alters ε from 0.0094 to 0.0076. Deformation conducted at lower temperature results in higher volume fraction of transformed particles of the same size compared to adequate deformation at higher temperature [6].

(4) Coherency loss induced by deformation.

As regards the observations conducted on deformed samples it was reported that increasing strain lowers the value of particle diameter for MT start [1, 7, 8]. The volume fraction of transformed particles in samples predeformed at room temperature and followed by cooling to 4.2 K is higher than that in only deformed samples [9]. It has been postulated that the MT of particle is initiated with the aid of the stress of glide dislocation [7]. In addition, the occurrence of secondary dislocations triggering the MT has been reported several times [10, 11]. The purpose of the present study is to examine the process of particle coherency loss during deformation and its further influence on the MT of γ-Fe particles. In the course of compression of Cu-Fe alloy single crystals, the distribution of dislocations in matrix generated

* *Permanent address:* University of Mining and Metallurgy, Division of Structure and Mechanics of Solid, 30-059 Cracow, Poland.

by deformation and at the vicinities of particles were observed by transmission electron microscopy (TEM). The particle size distribution in post-deformation annealed samples were established. The correlation between MT process and the change in particle size distribution is discussed.

2. Experimental details

Single crystal rods of 8 mm in diameter were grown from Cu-1.6 wt %Fe alloy by the Bridgman technique. The crystallographic orientation of rods axis was 4° apart from the [114] towards [011]. The crystals, cut to 10 mm in height, were solution-treated at 1273 K in evacuated capsules for 6 h and water quenched followed by aging at 973 K for 24 h. This produced coherent γ-Fe particles with an average diameter of 61 nm. The samples were compressed at 77 K at a strain rate of $1.7\times10^{-4}\,s^{-1}$ to shear strain (γ) from 0.003 to 0.17. For further examinations, the samples were cut in the middle sections along the sample axes. One halves were annealed at 773 K for 2 h in order to eliminate dislocations around particles induced by deformation and MT and therefore to allow the particle-size measurements. Second halves were bisected. One parts were chemically polished by the method described by Mitchell *et al*. [12], subsequently electropolished in 80% phosphoric acid at room temperature and slightly compressed to reveal slip events. The surfaces were examined by optical microscope with Nomarski contrast. Second parts were used for TEM observations of as-deformed state. Slices of about 500 μm thick were spark-cut from both kind of samples (as-deformed and annealed state) and chemically thinned [12] to a thickness of about 250 μm. These were dished by the jet polishing to less than 100 μm in thickness but before punching a hole. Final thin foils were obtained after electropolishing in 80% phosphoric acid at room temperature. The specimens were examined by JEOL 2000-FX electron microscope at 200 kV mounted in a double-tilt holder. The measurements of particle diameters were carried out with the accuracy of 0.2 mm from photographs of total enlargement of 1.4×10^6 times. For each deformation variant over 200 particles were measured.

3. Experimental results and discussion

The shear strain–stress curve is shown in Fig. 1. The black circles indicate the stages of structural examinations. Yielding started at stress of $\tau_0 = 14.5$ MPa.

3.1. Deformed state

3.1.1. Slip lines

The micrographs from surface observations are included in Fig. 1. It was observed that the lateral surface was covered with long, straight and randomly distributed primary slip lines in the initial stage of the deformation. In course of deformation, they become more prominent and densely distributed. At a strain of 0.03, faint traces of secondary (conjugate) system appear. Beyond strain of 0.09, traces of the primary slip boarder and become blurred while of the conjugate one becomes short and coarse operating within the band of the primary one. On micrograph from the last stage the traces of conjugate and critical planes lie in one direction on projection surface so it can not be determined which of them (or both) operate.

3.1.2. Transmission electron microscopy

The plastic deformation after yielding point (strain of 0.003) is related with very low density of primary dislocations (Fig. 2). They overcome particles by Hirsch mechanism [13] and generate rows of prismatic loops (Fig. 2a). Stacks of prismatic loops are emanating from one side of particles. Some of the γ-Fe particles are associated with attached dislocations and lobe contrast loss. Across the particles marked as A and B in Fig. 2b single dark lines can be resolved. Similar lines observed by Sato *et al*. [14] were interpreted as Orowan loops tightly bounded to the γ-Fe particles. However the traces of Orowan loops should be parallel to each other and to the trace of gliding dislocation because only the primary slip is active. Additionally each Orowan loop is related with one by-passing dislocation. In Fig. 2b line at particle A is perpendicular to line at particle B. At the larger particle (S) several lines extend in two perpendicular directions. The number of resolved traces at particle S is much higher than the density of dislocations in the matrix. Thus it is assumed that the discussed lines are the traces of dislocations generated at the γ-Fe particles interfaces in order to lower the misfit constrains turning them to semi-coherent ones.

The further straining to strain of 0.02 (Fig. 3) develops fairly homogenous distribution of primary dislocations. The lobe contrast on majority of particles disappears as they are surrounded by dislocations (Fig. 3a). However, some of them, especially smaller ones, are semi-coherent γ-Fe type. This is confirmed by the lobe contrast visible in the thinner part of foil where dislocations escaped to the foil surface (Fig. 3b). The larger particles (marked as T, Fig. 3d and e) are surrounded by complex arrays of dislocations which suggests that they had undergone martensitic transformation (refer to Section 3.2.2). In matrix, primary dislocations are often paired in stretched dipoles, which tend to lie in contact with particles. Such dipoles spreading on the cross glide planes are also resolved (arrowhead marks in Fig. 3c and d). Abrupt changes of direction in dislocation traces appear across conjugate and cross plane traces. It should be noticed that on Fig. 3a, c and d operating reflection is (111) and under the condition $\mathbf{b}\cdot\mathbf{g} = 0$ primary dislocations should be out of contrast. Nevertheless some dislocations on traces of primary plane are still visible. The general condition for a dislocation to be invisible requires additional equation given by $\mathbf{b}\cdot(\mathbf{g}\wedge\mathbf{u}) = 0$ to be fulfilled ($\mathbf{u}$ is the dislocation line direction). Here, for the primary dislocations of edge type, this condition is nonzero. Thus the visible dislocations may be the edge ones. The primary edge dipoles associated with particles and no presence of prismatic loops may suggest that by-passing obstacles is carried out by slightly modified Hirsch mechanism. The sketch is presented in Fig. 4f and the by-pass may proceed as follows: a part of dislocation gliding on the B primary plane

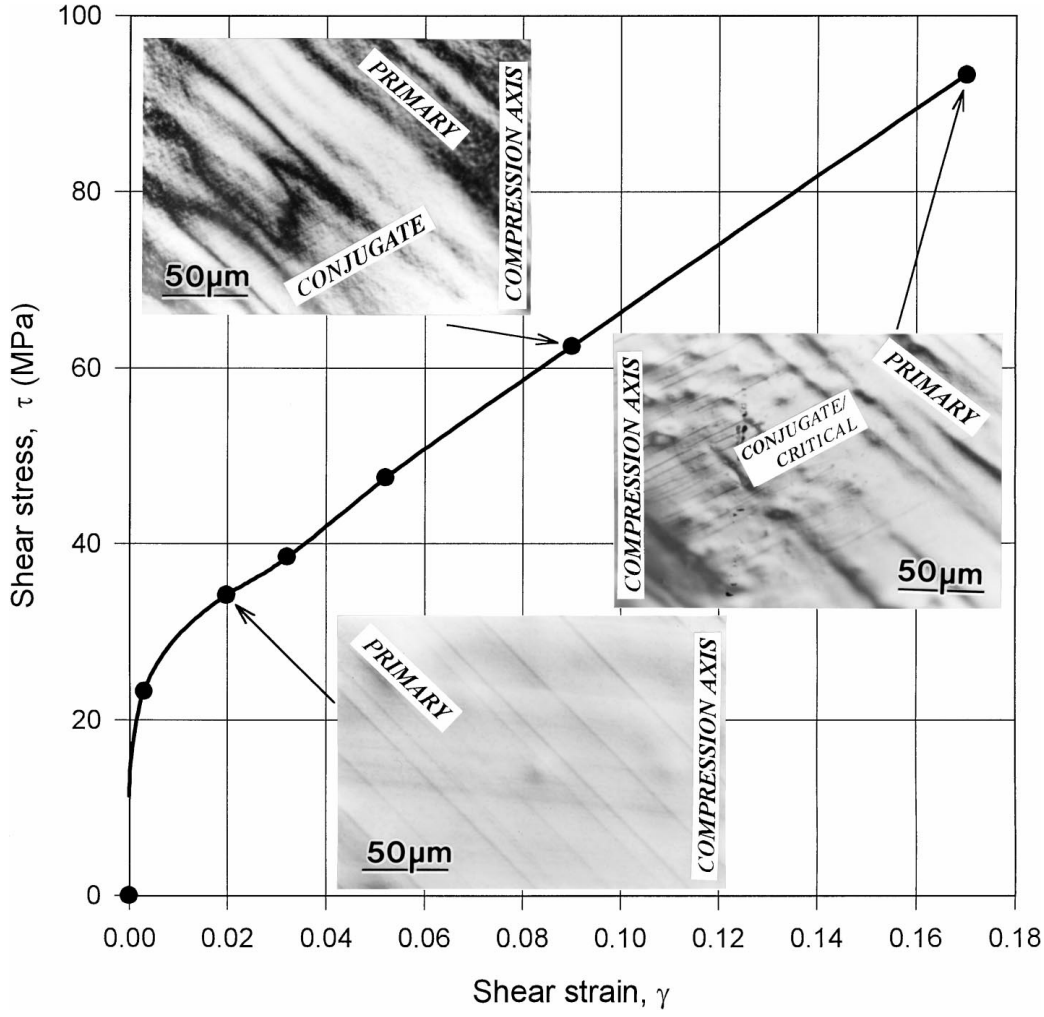

Figure 1 The compression shear stress–shear strain curve of copper–iron single crystal.

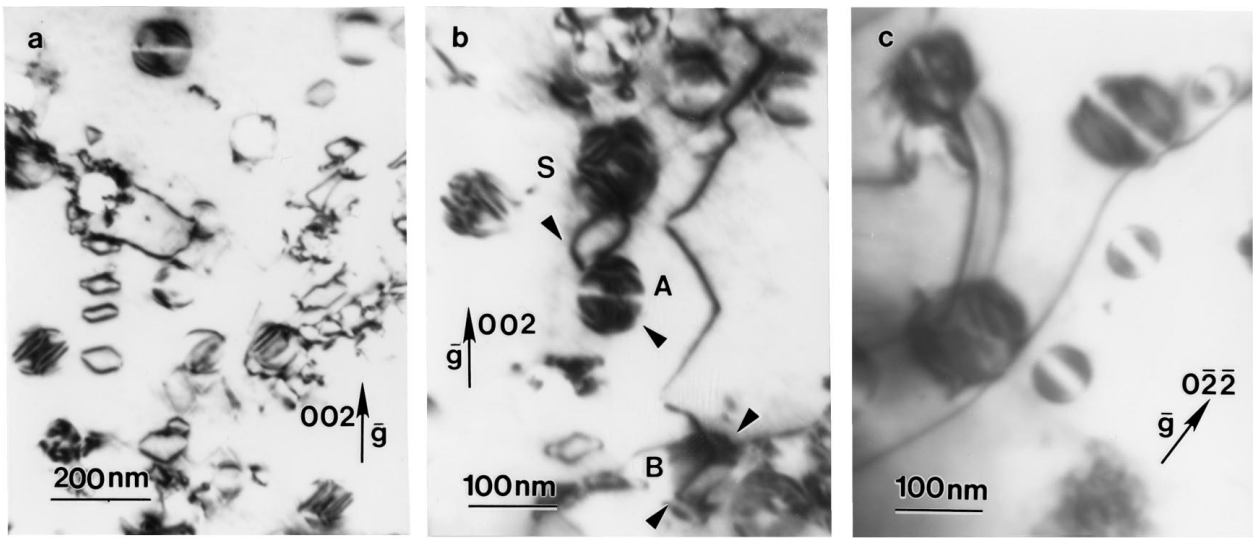

Figure 2 TEM structure of sample deformed to shear strain 0.003. (a) $\mathbf{g} = (002)$. Notice prismatic loops, (b) $\mathbf{g} = (002)$, (c) $\mathbf{g} = (0\bar{2}\bar{2})$. Traces of single dislocations are recognizable at particles marked A and B. Particle marked S is semi-coherent γ-Fe one.

double cross-slips onto B^* plane to overcome particle. After this maneuver, it further slides on B^*, stretching for longer distances and giving the observed image of dipoles in Fig. 3d and e.

With the process of straining, the density of long primary dislocations increases. Slip on secondary planes (conjugate and critical) becomes considerable active (above strains of 0.09). The substructure becomes more complex. Localized extensive tangling of secondary dislocations generated during MT occurs in the vicinity of transformed particles giving substantial contribution to cell walls formations (Fig. 4). The cell

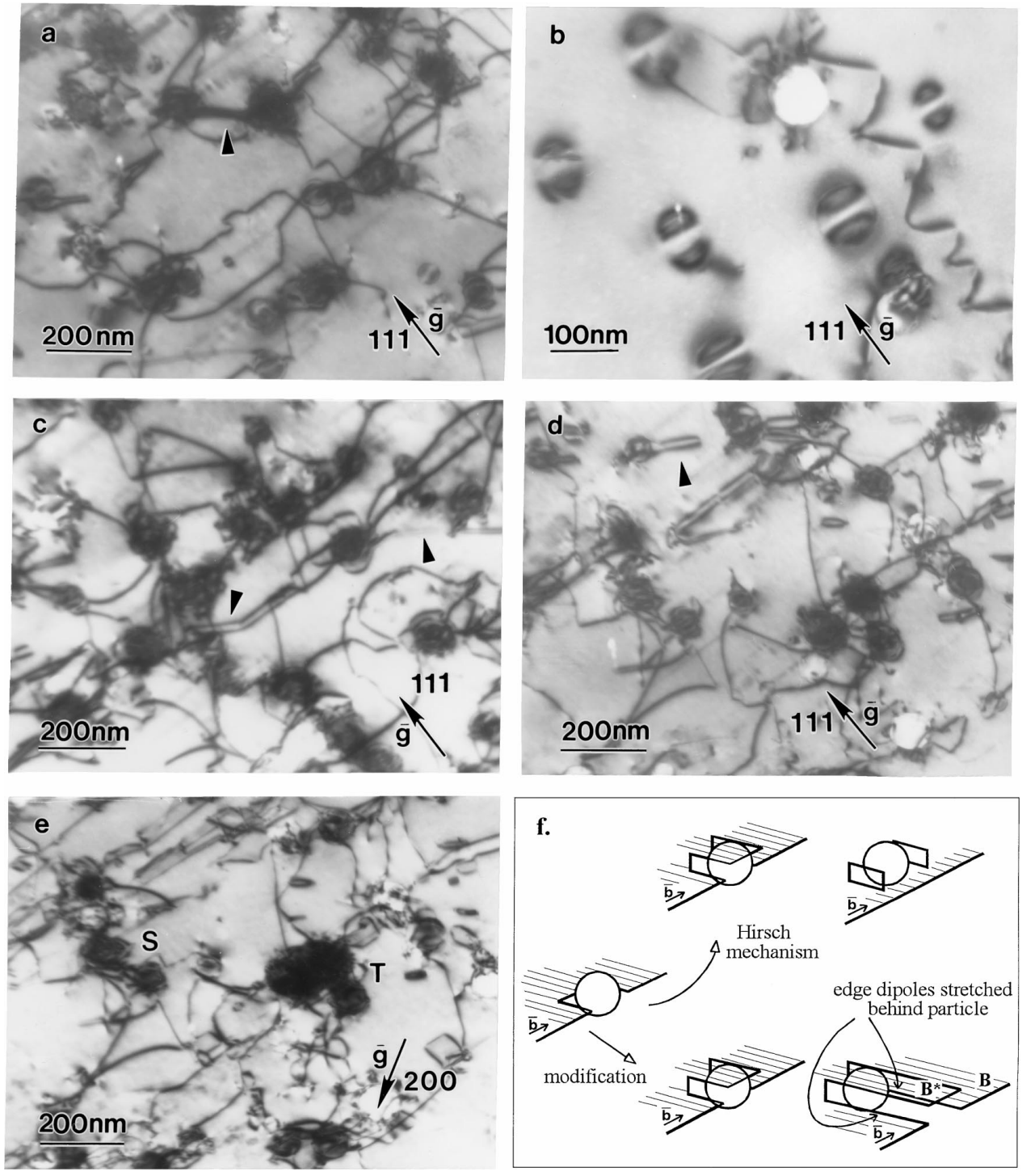

Figure 3 Stage of $\gamma = 0.02$. (a) Thicker part of foil showing particles surrounded by dislocations. $\mathbf{g} = (111)$, (b) Thinner part of foil revealing still coherent particles after dislocations escape, $\mathbf{g} = (111)$, (c) $\mathbf{g} = (111)$, (d), (e) This same view in $\mathbf{g} = (111)$ and $\mathbf{g} = (\bar{2}00)$, respectively. Arrowheads indicate short dipoles on cross plane; T and S indicate transformed and semi-coherent particles, correspondingly. (e) Scheme of modified Hirsch particle by-pass mechanism.

interiors are formed naturally as areas within the particles. The cells are comparable in scale with the spacing of particles. Nevertheless the revealed cell structure is not as distinct as that in pure Cu. Particles appear to inhibit the development of the cell structure. Similar influence of particles on generation and distribution of dislocations was reported in fatigue of Cu-Fe alloy single crystals [15]. Accumulations of dislocations do not have a tendency to be aligned in layers along the traces of any particular slip plane as it is reported for Cu single crystals [16] and Cu single crystals with second phase particles [10, 13].

3.2. Post-deformation annealed state

3.2.1. Transmission electron microscopy

The TEM examples of the post-deformation annealed structure for various steps of deformation are shown in Fig. 5. In the micrographs, three types of particles may be easily resolved. One is martensiticly transformed

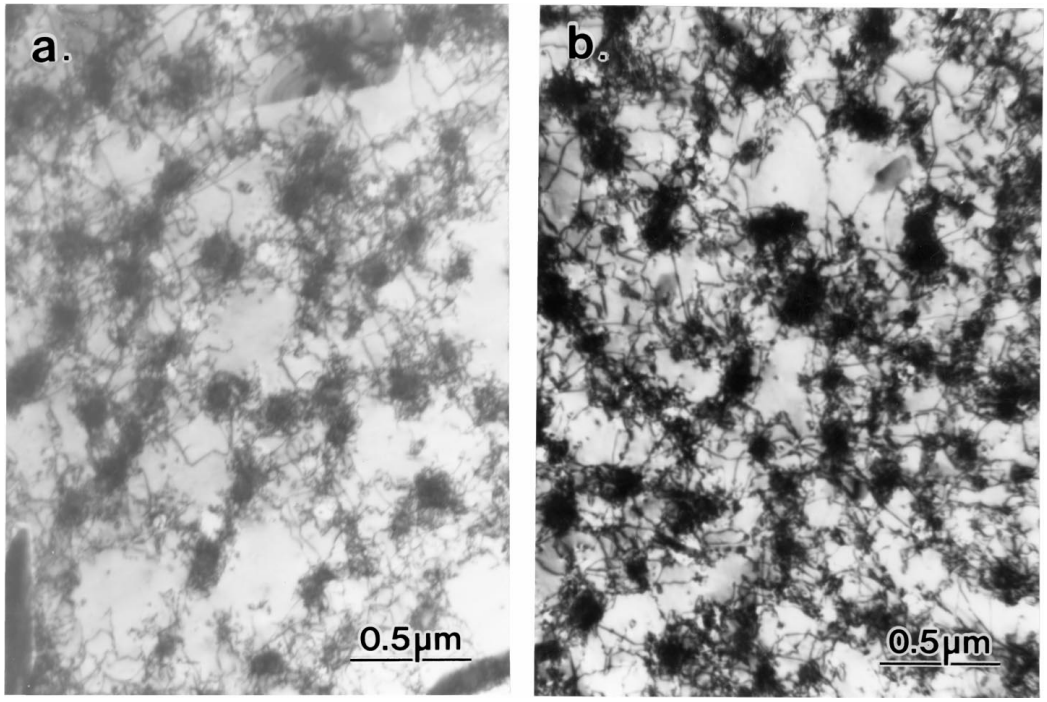

Figure 4 Stage of (a) $\gamma = 0.09$, $\mathbf{g} = (1\,\bar{1}\,1)$; (b) $\gamma = 0.17$, $\mathbf{g} = (0\,\bar{2}\,0)$.

α-Fe particles observed as ellipsoid, black and uniform images (marked as T). The others are two kinds of γ-Fe particles: coherent and semi-coherent ones (marked C and S, respectively). By coherent it is meant that there is one-to-one correspondence between atoms at the particle-matrix interface. These particles are characterized by the non-contrast line perpendicular to the operating vector **g**. Semi-coherent means local non-conservation at lattice sites across the interface, the particles are surrounded by numerous interface dislocations. It should be noticed that annealing process does not change the image of semi-coherent particles compared with the as-deformed images. Different reflecting conditions cause subsequent changes of the dislocation pattern in the semi-coherent particle interface. An example is shown in Fig. 6. It may be seen that matrix dislocations belong to the (111) primary (B) and $(\bar{1}\,\bar{1}\,1)$ conjugate (C) slip planes. The interface of coarser semi-coherent particle (marked as S_4) is composed of complicated dislocation network with several Burgers vectors. The interesting feature appears at finer particles named S_2 and S_3, where only few interface dislocations are resolved. These semi-coherent particles observed in $\mathbf{g} = 220$ reflection are visible with lobe contrast which is characteristic for the coherent particles. The effect is due to the absence of displacements in reflecting plane caused by the interface dislocations and is possible when the dislocation Burgers vector is $[1\,\bar{1}\,0]$. This observation coincides with the formal analysis of the dislocation structure at interfacial boundaries presented by Christian [17]. In the particular case of a semi-coherent boundary with a small misfit between planes lying normal to the boundary, the dislocation structure is an array of parallel edge dislocations with their Burgers vector lying in the boundary plane. Thus, at least at the (110) plane still good fit between particle and matrix lattices exists. The details of the dipole formation during the by-pass of S_2 particle by B5 slip system dislocation, according to the modification proposed in Fig. 3f, may be revealed. By-passed dipole starts moving on the conjugate plane.

The three kinds of particles were also examined by diffraction in the converged beam mode. The diffraction patterns are presented in Fig. 7. Reflections from coherent particle are very sharp and distinct (Fig. 7a). New reflections from b.c.c. structure appear in the pattern taken from martensiticly transformed particle (Fig. 7c). In contrast, reflections from semi-coherent particle (Fig. 7b) are almost similar to those in Fig. 7a, but diffuse due to the accumulated interface dislocations.

3.2.2. Particle size measurements

The progress of MT in particles by straining was examined in annealed samples and the fraction of transformed particles against shear strain is plotted in Fig. 8. Additionally the Fe particle sizes and their distribution were examined. Fig. 9, where coherent and semi-coherent γ-Fe particles are plotted separately, shows their frequency distribution histograms and the changes in the particles mean diameter with strain. On statistical distributions graphs, width of interval is constant and equals to 10 nm. It is clearly noticed that the diameters of coherent particles are smaller than that of semi-coherent ones at all strains. Fig. 9 also indicates the critical diameter for coherency loss of particle. This is given by an average value of the maximum diameter of coherent particles and the minimum one of semi-coherent ones at each strain. The critical diameters for coherency loss are ranged from 50 to 58 nm.

Fig. 10a–g show the change in the size distribution of the γ-Fe and α-Fe particles with strain. Both γ-Fe

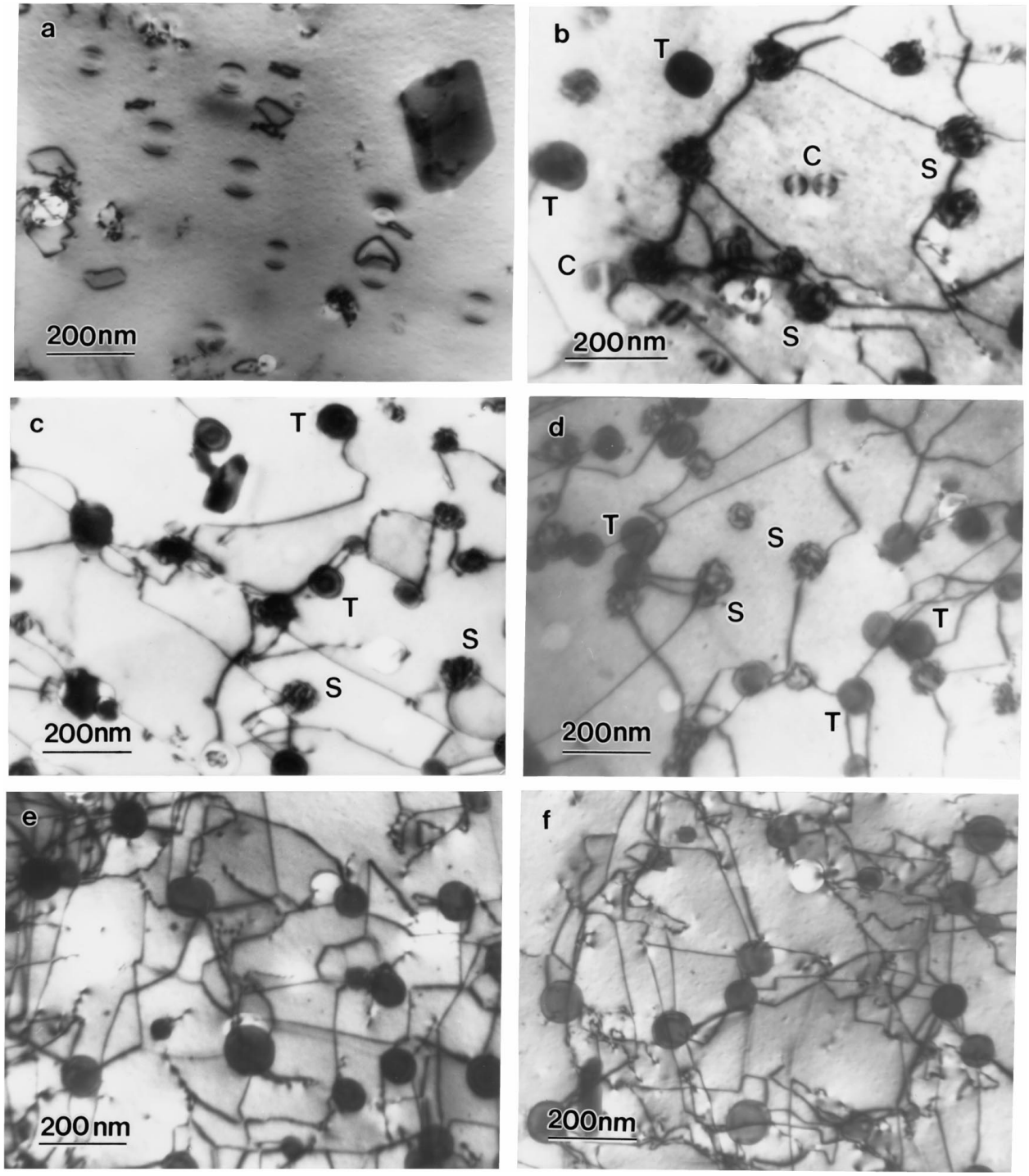

Figure 5 TEM observations of post-deformation annealed structures. (a) $\gamma = 0.003$, (b) $\gamma = 0.02$, (c) $\gamma = 0.03$, (d) $\gamma = 0.05$, (e) $\gamma = 0.09$, (f) $\gamma = 0.17$. T indicate MT α-Fe particles, C and S coherent and semi-coherent γ-Fe particles, respectively.

coherent and semi-coherent particles were treated as coherent ones. The distribution of γ-Fe particles becomes narrower with strain and it can be seen that the early stages of deformation are associated with the MT mainly within the large γ-Fe particles. This is more clearly shown in Fig. 10h where changes in the particle mean size and its standard deviation with strain are presented. It is noted that the mean diameter and standard deviation of γ-Fe particles drop with the start of straining because of the $\gamma \rightarrow \alpha$ transformation taking place in coarser particles. In contrast, an increase in the standard deviation of α-Fe particles is clearly prominent at strains above 0.05. The mean diameter of these particles decreases at small strains and then approaches a constant value. This indicates that MT takes place in smaller γ-Fe particles at strains above 0.05. Present observations that MT starts within coarser γ-Fe particles while finer particles need higher strains to execute the MT are in qualitative agreement with results by Monzen *et al.* [8] and Matsuura *et al.* [10].

3.3. Conditions for particle coherency loss

One of the assumptions why dislocation nucleates at the particle interface may be derived from purely geometrical considerations of lattice misfit between two

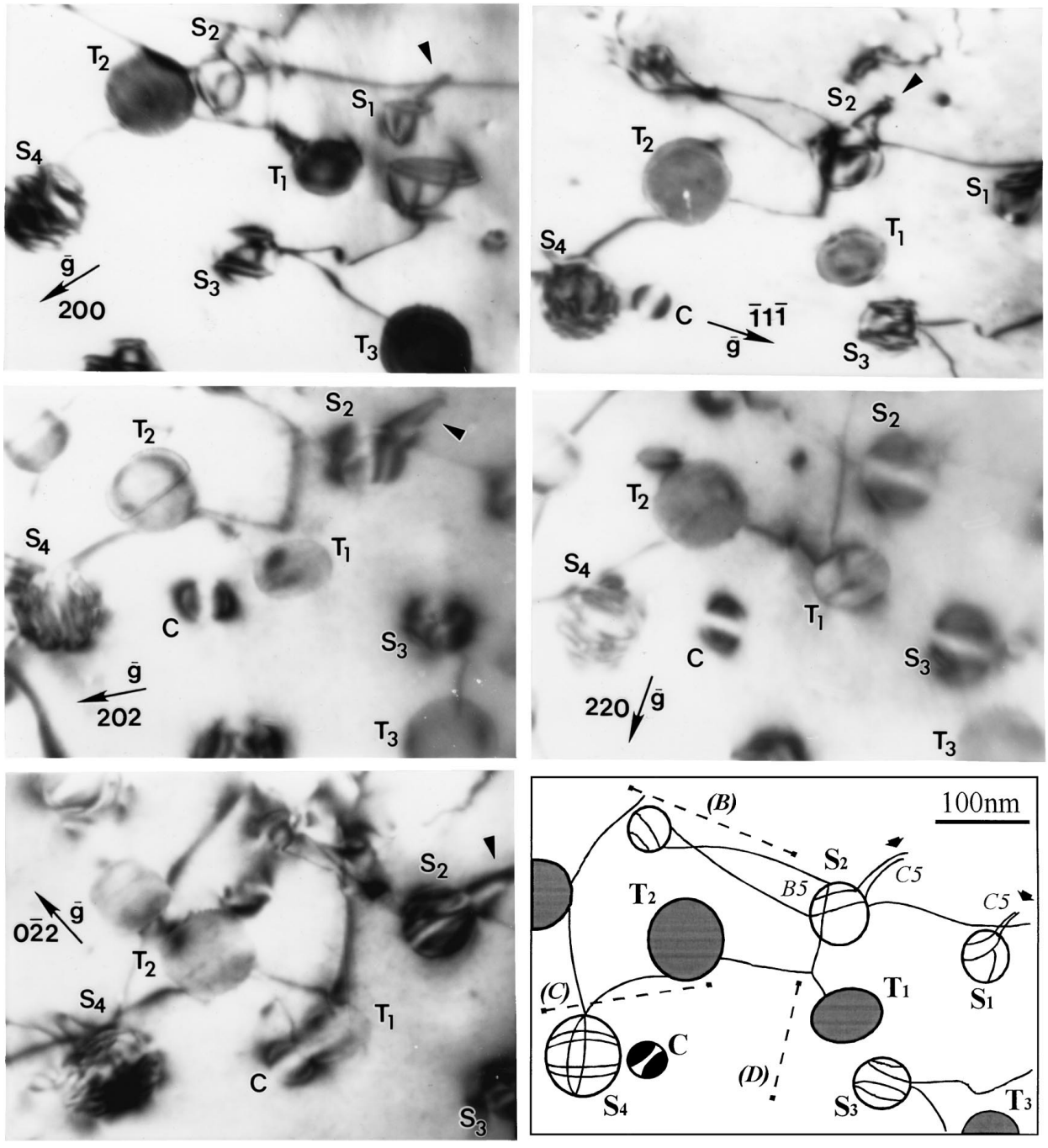

Figure 6 Coherent (C), semi-coherent (S) and transformed (T) particles analyzed in different operating reflections in sample annealed after deformation to $\gamma = 0.02$. Directions of slip plane traces and designations of slip systems are marked on the sketch. Arrowheads indicate places of cross-slip dipoles formation.

coherent phases. The number of extra planes (dislocations) n to be accommodated by material with smaller interplanar spacing in radius distance r is:

$$n = \frac{r}{d_\mathrm{p}} - \frac{r}{d_\mathrm{m}} = \frac{d_\mathrm{m} - d_\mathrm{p}}{d_\mathrm{p} d_\mathrm{m}} r,$$

where d_m and d_p are lattice parameters of matrix and particle, correspondingly. From this simple geometric argument one can notice that the larger particle is the more dislocations appear at the interface. From above equation the critical radius r_ε for one dislocation generation ($n = 1$) is given by:

$$r_\varepsilon = \frac{d_\mathrm{p} d_\mathrm{m}}{d_\mathrm{m} - d_\mathrm{p}}$$

and for $d_\mathrm{m} = 0.3607$ nm, $d_\mathrm{p} = 0.3562$ nm [18] we obtain $r_\varepsilon = 28.55$ nm ($d_\varepsilon = 57.1$ nm). Brooks gave the formula of spacing t between the interface dislocations [19]:

$$t = \frac{d_\mathrm{p} + d_\mathrm{m}}{2(d_\mathrm{p} - d_\mathrm{m})} |\mathbf{b}|,$$

which for perfect dislocation a/2⟨110⟩ type gives the value of 20.3 nm. The values of critical diameter obtained in the present experiment (Fig. 8) are ranged from 50 to 58 nm and the distinguishable dislocation spacing at the particle interface for strain 0.003 varies between 22 and 28 nm. Both results are in good agreement with above calculations. Similar considerations were conducted by Weatherly and Nicholson [20] and reported

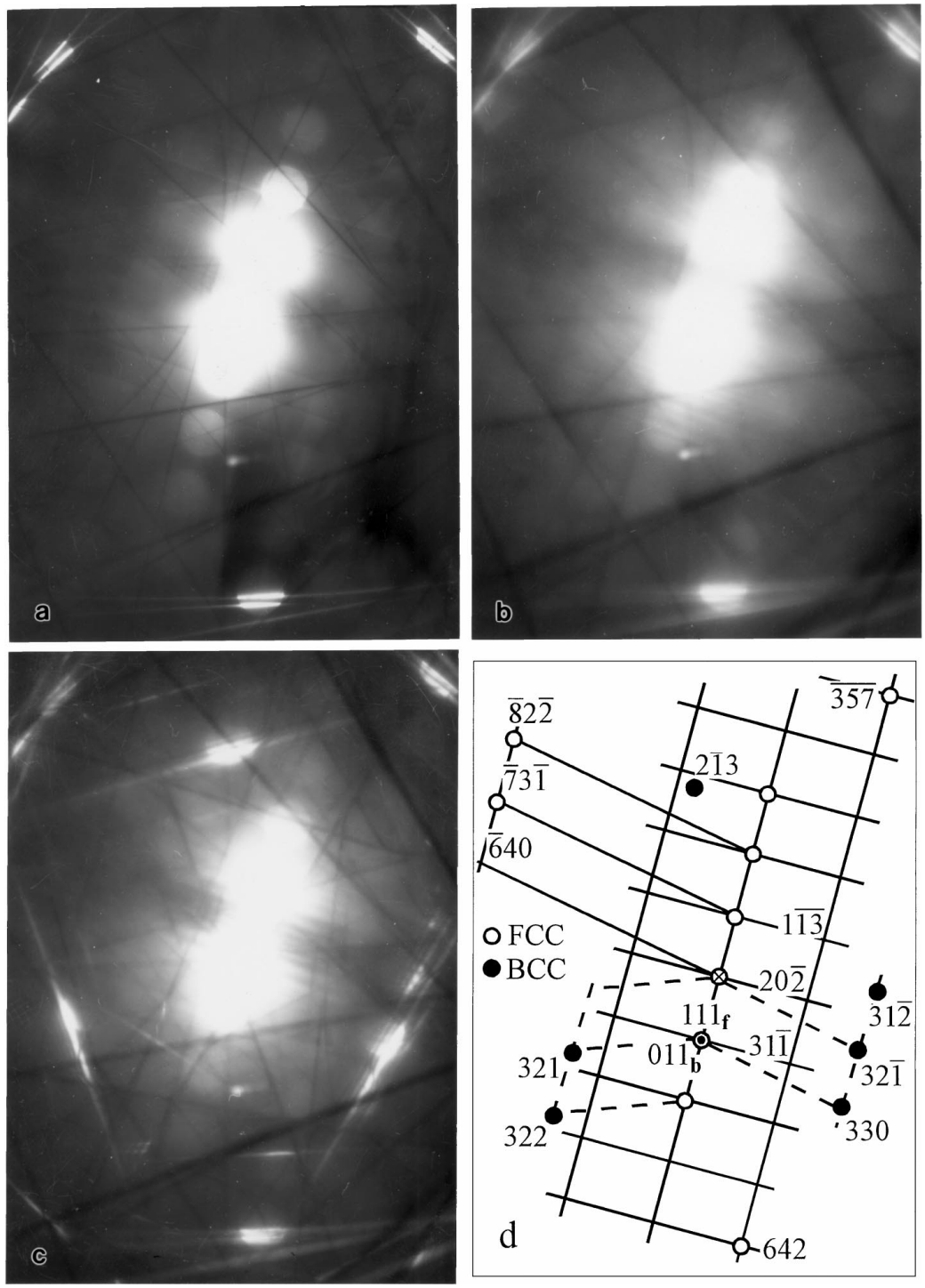

Figure 7 CBED from (a) coherent γ-Fe particle, (b) semi-coherent γ-Fe particle and (c) MT α-Fe particle, (d) Index from diffraction spots.

that spacing of dislocations on the interfaces of spherical γ' particles in Nimonic alloy was similar to the value calculated from the known misfit of the two lattices. Presented considerations are statical and do not take into account the influence of stress field of moving dislocation. Nevertheless they provide a rough explanation for evidence of coherency loss within coarser particles.

As stated above, there should be more probable for particle to lose coherency as its diameter increases. It was shown [21], that the measurement of image widths of strain fields around coherent particles observed in TEM can yield information about the magnitude of strains. This is also the most effective method of studying particle coherency [22]. If the particle loses coherency the value of strain ε measured of the direction parallel to **b** will be reduced compared to the initial value for fully coherent particle. Thus on the plot of measured value of strain ε against particle size the loss of coherency should be manifested by drop on the plot. This kind of plot is presented on Fig. 11 plotted for 40 randomly chosen γ-Fe particles of initial stage. It may be seen the sudden drop of coherency strains for diameter about 35 nm which deteriorates with the particle size. The number n of created dislocations of Burgers vector **b** may be assessed by formula $\Delta\varepsilon = n\mathbf{b}/r$, where $\Delta\varepsilon$ is the difference of coherent and measured

strains for particle of given radius r [22]. From present measurements for the particle of $d = 60$ nm one perfect dislocation a/2⟨110⟩ type may be created.

It is known that the elastic energy of a coherent precipitate is proportional to the volume of the precipitate,

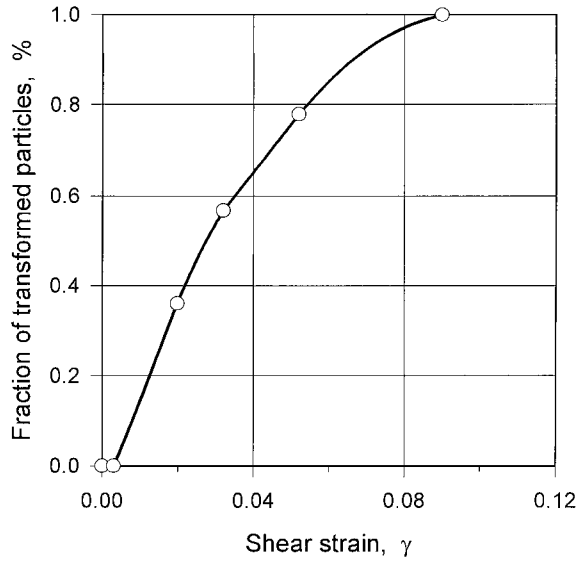

Figure 8 Fraction of transformed particles.

whereas the elastic energy of a semi-coherent one is proportional to the area of interface [19]. It follows that will be a critical size, above which the semi-coherent state will have the lower energy. Thus the particle will have a tendency to lose coherency, but due to the misfit constrains it cannot of itself do so. A major disruption of the lattice in its neighborhood (passing dislocation or irradiation) may cause it to generate interface dislocations. There exist in literature calculations for critical particle radius for loss coherency, which are based on the energetic considerations of interaction energies of a dislocation and a particle [23–25]. Those energy-based criteria are strongly particle size dependent. In the previous paper [26] the critical diameter for two prismatic loops generation during the interaction of moving dislocation was calculated to be 60.8 nm. The calculated value lies within the observed range.

Presented results indicate the possibility of deformation induced coherency loss of γ-Fe particles prior to the martensitic transformation. The present investigation can not provide clear description of the MT mechanism. However the one presented by Monzen and Mori [7] which assumes the aid of the stress of glide dislocation is not contradicted with present observations.

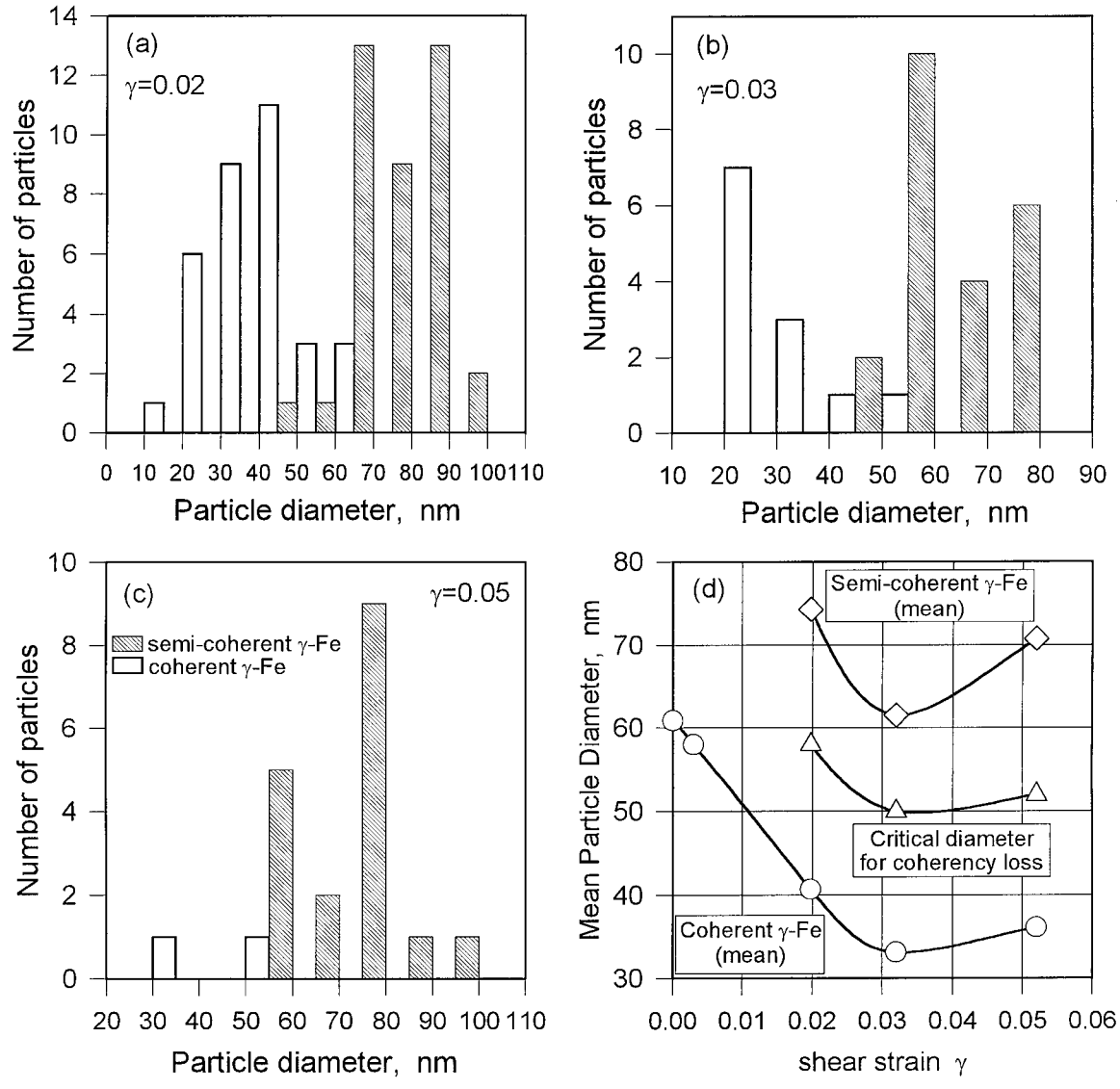

Figure 9 Coherent and semi-coherent γ-Fe particles. (a), (b), (c) diameter frequency distribution histograms for $\gamma = 0.02$, $\gamma = 0.03$ and $\gamma = 0.05$, respectively, (d) variation of the mean diameter and the critical diameter for coherency loss with strain.

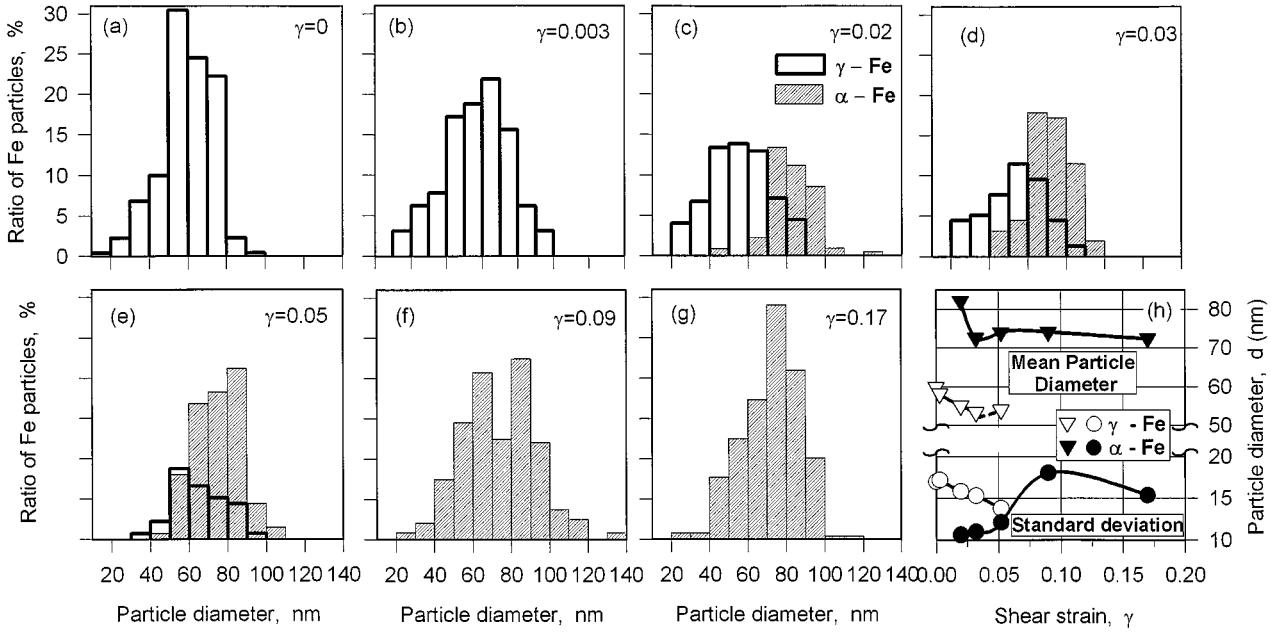

Figure 10 (a–g). The change in the diameter frequency distribution histograms and (h). Variation of mean diameter and standard deviation of the γ-Fe and α-Fe particles with strain.

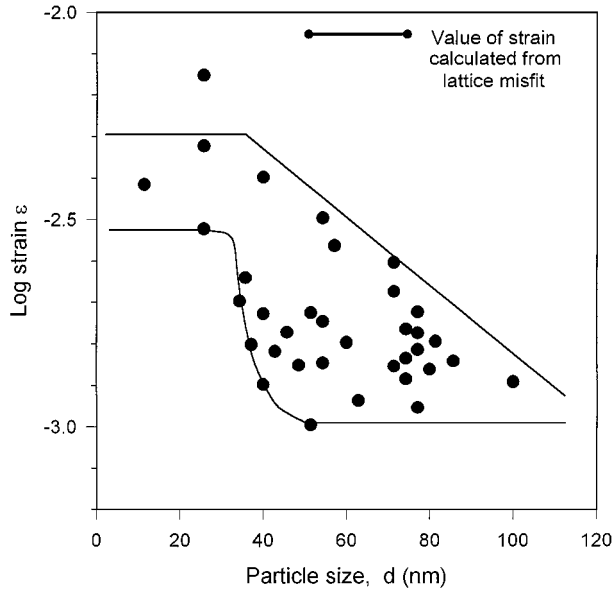

Figure 11 Experimental value of misfit strain ε against coherent γ-Fe particle diameter. Initial stage.

4. Conclusions

Deformation induced martensitic transformation in γ-Fe particles was investigated during compression in liquid nitrogen and main conclusions may be summarized as follows:

1. The dislocations are fairly and homogeneously distributed in sample. The cell structure is not evolved as distinct as one developed during deformation of pure copper. Accumulations of dislocations are not arranged in layers, which is also on the contrary with the structure developed in pure copper. The presence of particles inhibits the evolution of structure.

2. The stretched dipoles, which tend to lie in contact with particles were revealed. It is supposed they were formed during particle by-pass and therefore the modification to the Hirsch mechanism has been proposed.

3. In process of deformation three kinds of particles were resolved, namely coherent and semi-coherent (f.c.c. type) and martensiticly transformed (b.c.c. type). The critical diameter for coherency loss was found to be 58 nm at initial stage decreasing with strain to 50 nm. Observed values are in good agreement with the ones calculated by statical and energetical formulas for coherency loss.

4. The interaction of a primary dislocation with a coherent γ-Fe particle seems to be not enough to trigger the martensitic transformation. The additional factor for particle transformation is relaxation of constrains from the surrounding matrix by loosing coherency. The MT is most probably triggered by the interaction of semi-coherent particle with the glide dislocation. The coherency loss is strongly particle size dependent (the larger particle the easier coherency loss) and this phenomenon may explain the particle size dependency of MT.

Acknowledgements

One of the authors (A. M. W.-S.) would like to express thanks to Prof. M. Niewczas for his helpful advice in thin foils preparation.

References

1. K. E. EASTERLING and H. M. MIEKK-OJA, *Acta Metall.* **15** (1967) 1133.
2. K. R. KINSMAN, J. W. SPRYS and R. J. ASARO, *ibid.* **23** (1975) 1431.
3. G. R. WOOLHOUSE, *Phil. Mag.* **28** (1973) 65.
4. A. SATO, N. ISHIKAWA and T. MORI, *Mat. Sci. Eng.* **81** (1986) 427.
5. Y. WATANABE, M. KATO and A. SATO, *J. Mater. Sci.* **26** (1991) 4307.

6. R. MONZEN, A. SATO and T. MORI, *Trans. Jap. Ins. Met.* **30** (1989) 359.
7. R. MONZEN and T. MORI, *Acta Metall. Mater.* **43** (1995) 1451.
8. R. MONZEN, A. SATO and T. MORI, *Trans. Jap. Ins. Met.* **22** (1981) 65.
9. Y. WATANABE and A. SATO, *Scripta Met.* **23** (1989) 359.
10. K. MATSUURA, M. TSUKAMOTO and K. WATANABE, *Acta Met.* **21** (1973) 1033.
11. N. ISHIKAWA and A. SATO, *Phil. Mag.* **A 64** (1991) 387.
12. J. W. MITCHELL, J. C. CHEVRIER, B. J. HOCKEY and J. P. MONAGHAN, Jr., *Can. J. Phys.* **45** (1967) 453.
13. F. J. HUMPHEYS and P. B. HIRSCH, *Proc. Roy. Soc. Lond.* **A 318** (1970) 73.
14. A. SATO, M. MORI and T. MORI, *Trans. Jap. Ins. Metals* **25** (1984) 863.
15. M. KATO, N. HONJO and T. FUJII, *ISIJ Int.* **37** (1997) 1224.
16. S. J. BASINSKI and Z. S. BASINSKI, in "Dislocation in Solids," edited by F. R. N. Nabarro, (North-Holland, 1979) p. 263.
17. J. W. CHRISTIAN, "The Theory of Transformations in Metals and Alloys," Part I, 2nd edition (Pergamon Press, Oxford, 1978) p. 359.
18. Z. S. BASINSKI, W. HUME-ROTHERY, F. R. S. and A. L. SULLON, *Proc. R. Soc. Lond.* **A 229** (1955) 459.
19. H. BROOKS, "Metal Interfaces" (ASM, 1962) p. 20.
20. G. C. WEATHERLY and R. B. NICHOLSON, *Phil. Mag.* **17** (1968) 801.
21. M. F. ASHBY and L. M. BROWN, *ibid.* **8** (1963) 1083.
22. P. HIRSCH, A. HOWIE, R. NICHOLSON, D. W. PASHLEY and M. J. WHELAN, "Electron Microscopy of Thin Crystals," 2nd edition (Krieger Publisher, FL, 1977) p. 350.
23. M. F. ASHBY and L. JOHNSON, *Phil. Mag.* **20** (1969) 1009.
24. L. M. BROWN and R. K. HAM, in "Strengthening Methods in Crystals," edited by A. Kelly and R. B. Nicholson (Elsevier, 1971) p. 9.
25. L. M. BROWN and G. R. WOOLHOUSE, *Phil. Mag.* **21** (1970) 329.
26. A. M. WUSATOWSKA-SARNEK, H. MIURA and T. SAKAI, *Scripta Met.* **39** (1998) 1457.

Received 9 December 1998
and accepted 20 April 1999